of voids. A rough surface was simulated by applying a mathematically defined function to allow for light scattering that occurs from the surface of the material, considering that scattering is higher at longer wavelengths than at shorter wavelengths. It is also worth mentioning that underneath the rough surface a thin silicon oxide layer was defined to account for surface oxidation effects.

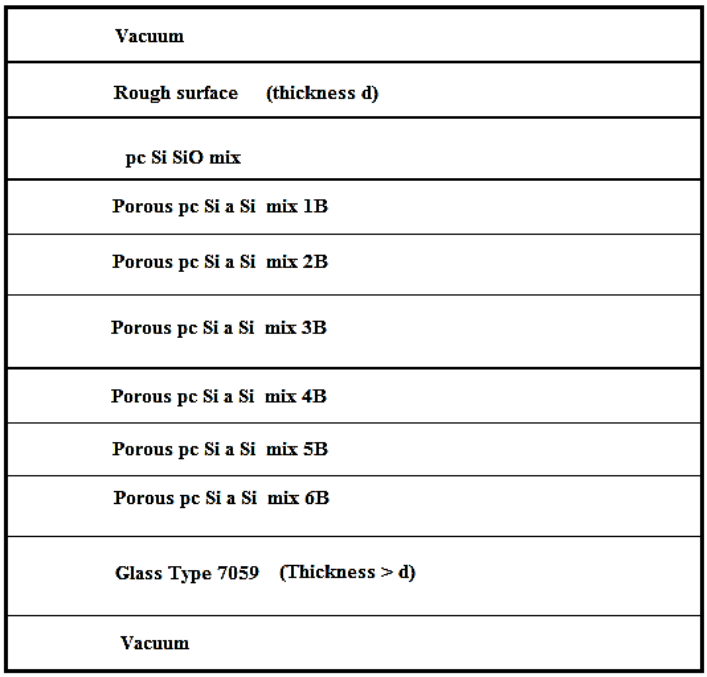

Figure 4.7: Virtual layer stack consisting of voids and a rough interface correction with the scattering formula for surface features.

4.13.2 SELECT THE FIT PARAMETERS

After the definition of all optical constants and layer stacks, the spectrum was loaded, and the fit parameters were defined. The simulation of the spectrum was then executed, and the software could adjust the fitting parameters by default to reach optimal agreement between

simulation and measurements. The program calculates the simulated R and T spectra together with the associated optical constants over the specified energy range. The program then changes the initial fit parameters and calculates new R and T spectra such that if the comparison with the measured spectra results in a smaller deviation, then the program replaces the initial fit parameters. This iterative process was repeated until no further improvement of the deviation can be achieved. It was also necessary to adjust the parameters manually in a case where the fit was not good enough in order to bring the simulation 'closer' to the data, from which the automatic fit then proceeded again. The goodness of fit value was expressed as the deviation of the simulated spectra from the measured spectra and the values of goodness of fit for various categories are given as indicated in table 4.1. The virtual layers are only used in the model, the absorption coefficient, film thickness, energy band gap and refractive index values for the complete real film are extracted from the model using the theoretical equations derived earlier in this chapter.

Table 4.1 Rating classification levels according to the deviation of the simulation from spectra.

Rating description	**Excellent**	**Good**	**Acceptable**	**Bad**	**Rejected**
Value	10^{-5}	10^{-4}	10^{-3}	10^{-2}	10^{-1}

4.14 RESULTS AND DISCUSSION

4.14.1 MEASURED AND SIMULATED SPECTRA

Figure 4.8 and Figure 4.9 present the measured and simulated transmittance spectra of the two nanocrystalline thin films deposited at 95% and 81.7% hydrogen dilutions respectively. The

transmittance intensities in the y-axis are reported in absolute values i.e. $\frac{T}{100}$. Due to internal multiple reflections occurring within the film, the interference patterns are observed.

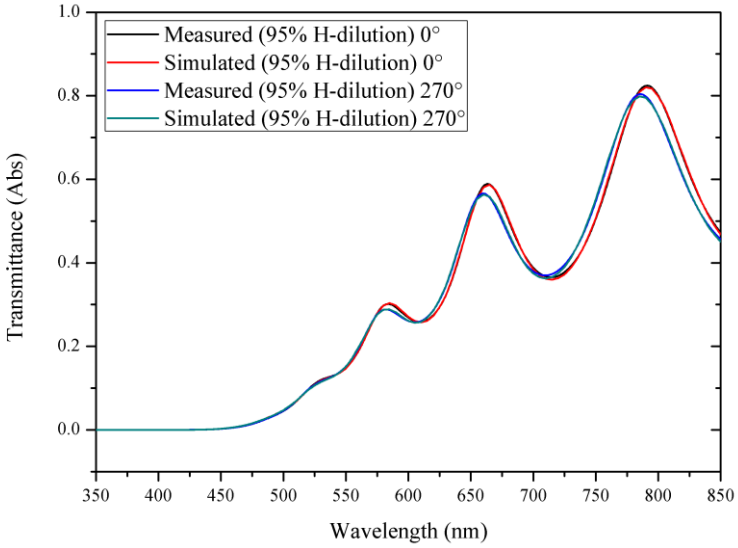

Figure 4.8: Measured and simulated transmittance spectra at 95% hydrogen- dilution.

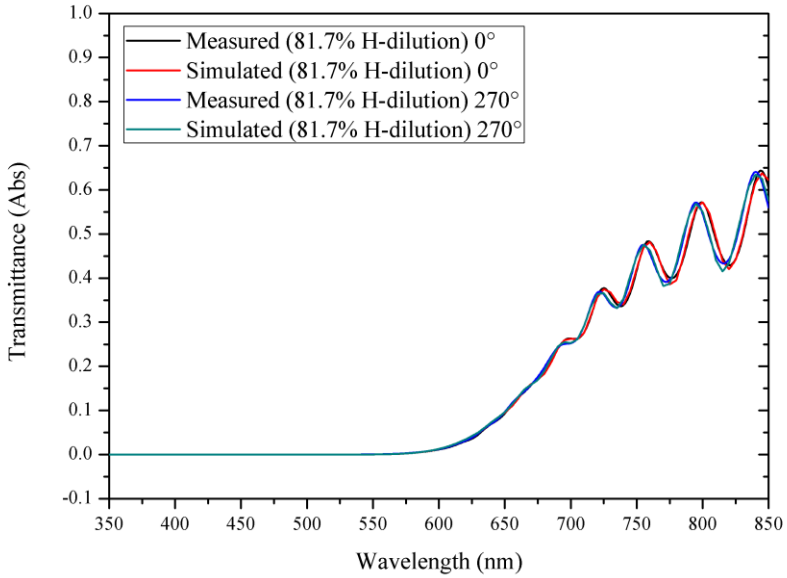

Figure 4.9: Measured and simulated transmittance spectra for a) 81.7% Hydrogen- dilution.

From the interference patterns of the two films, one can immediately predict visually whether the sample is thick or thin. The interference patterns of a thin sample are spread far apart from each, while for a relatively thick sample are closely spaced. Thus, from visual assessment, the nanocrystalline film deposited at 95% hydrogen dilution is thinner relative to the film deposited at 81,7 %. It is also evident that no transmission is observed from the wavelength of <450 nm and <600 nm in the respective transmittance spectra, which implies that the light is completely absorbed in these regions. The cut-off for strong light absorption occurs at different wavelength for the two respective spectra i.e. at λ=450 nm and λ = 600nm for 95% and 81.7% hydrogen dilution respectively. The blue shift in absorption with increased hydrogen dilution is related to the domination by the quantum confinement effect on the optical properties of nc-Si:H deposited at 95% hydrogen dilution [4.40]. The results from XRD and Raman has confirmed the increased in crystalline volume fraction and enhanced crystallinity at high hydrogen dilution. As the number of nanosized crystallites increase, the electronic density of state is decreased and expected to reduce the absorption coefficient values of the material.

Beyond the cut-off for strong absorption i.e. at approximately λ > 450 nm for 95% hydrogen dilution and λ > 600 nm for 81.7% hydrogen dilution, a gradual increase in transmittance is observed. A very small portion of light is absorbed, and the film is almost transparent. The absence of absorption in this region is attributed to the fact that photons have insufficient energy to cause electronic transitions from the valence band to a higher energy state. The transmittance for the respective films increases gradually to a maximum value of 0.8 and 0.6 respectively.

Figure 4.10 and figure 4.11 present the measured and simulated specular reflectance spectra of the two nanocrystalline thin films at 95% and 81.7% hydrogen dilutions respectively. When the transmittance and reflectance spectra of the respective nanocrystalline thin films are compared, a drop in both transmittance and specular component is observed. This is attributed to the surface roughness. AFM has confirmed that the nanocrystalline thin film deposited at 81.7% has a higher (rms) roughness value which is agreeing with the observation.

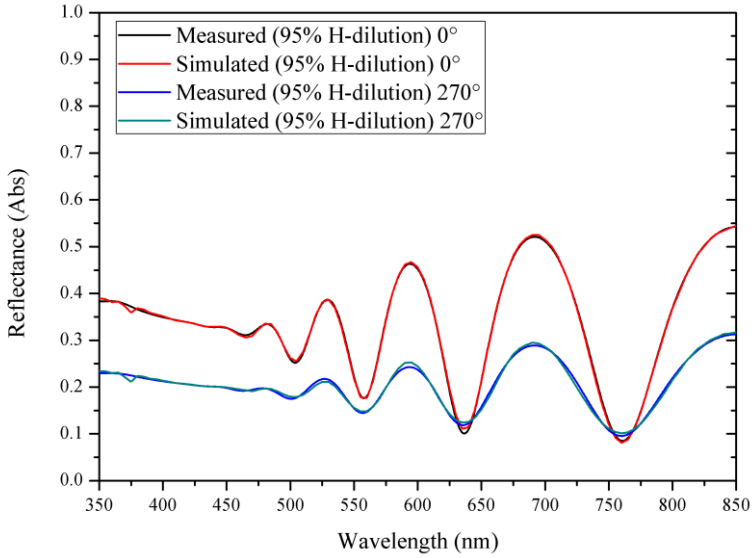

Figure 4.10: Measured and simulated specular reflectance spectra at 95% Hydrogen-dilution.

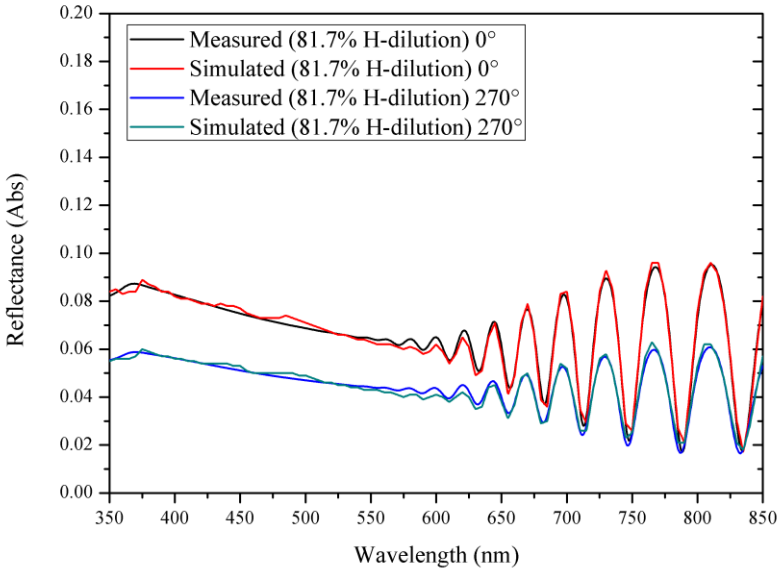

Figure 4.11: Measured and simulated specular reflectance spectra at 81.7% Hydrogen – dilution.

Another interesting feature is observed when the sample is rotated from 0° through to 360°, ensuring that the incident beam is maintained at the same spot. The results (not shown) reveals that the shape of both reflectance and transmittance spectra (i.e. measured at 90° and 180°) of nanocrystalline thin film deposited at 81.7% appears distorted and the intensity decrease to a level where it is difficult to perform the simulation. This behaviour is attributed to the orientation of the crystallites with respect to the incident light. Thus, rotating the sample places the crystallites at various positions relative to the incident beam. As a result, the incoming light interacts differently with the material. Additionally, some of the orientations scatter or transmit light more relative to the other and in some instances, the spectra appear to be distorted which makes the fitting of the spectra difficult, more especially for the thicker sample. To avoid this limitation, transmittance and reflectance spectra at “0°” and “270°” rotations were used for the fitting to determine the optical constants.

Contrary to the transmittance spectra, for high energies, where absorption is high the intensity of the specular reflected light increases. Since light is scattered by particles that are smaller than the light wavelength, the shorter wavelength is scattered much more than the longer wavelengths, which result in an increased intensity of the reflectance. In fact, when the reflectance spectra of nc-H:Si thin films are compared with the c-Si reflectance spectra, it can be seen that *nc*-H:Si thin film deposited at 95% hydrogen dilution approximate the c-Si spectra better that the *nc*-H:Si thin film deposited at 81.7% in this region confirming that *nc*-H:Si thin film deposited at 95% is more crystalline.

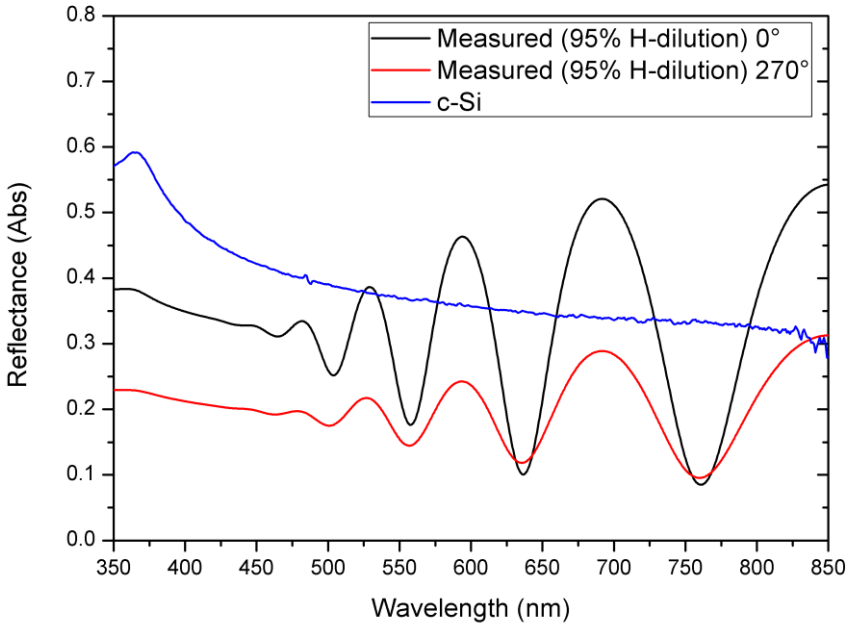

Figure 4.12: Comparison of measured specular reflectance spectra with c-Si.

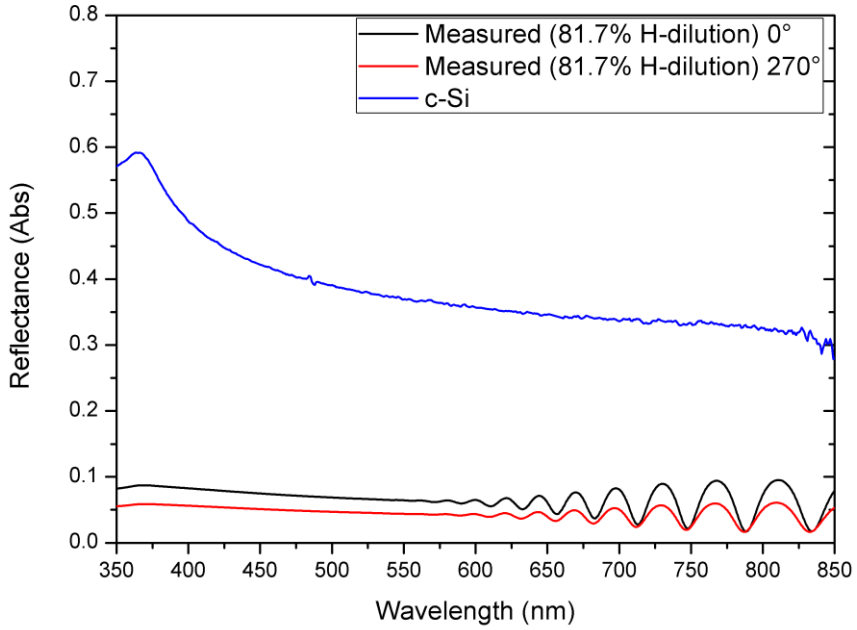

Figure 4.13: Comparison of measured specular reflectance spectra with c-Si.

4.14.2 DETERMINATION OF ABSORPTION COEFFICIENT

Light traveling in an absorbing medium is attenuated. The attenuation of the medium is related to the absorption coefficient (α). A plot of absorption coefficient as a function of energy shows high values in the high-energy region and low values as it approaches the low-energy region. The spectral dependence of the absorption coefficients α(*v*) calculated from the transmittance spectrum at "0°" and "270°" is depicted in Figure 4.14.

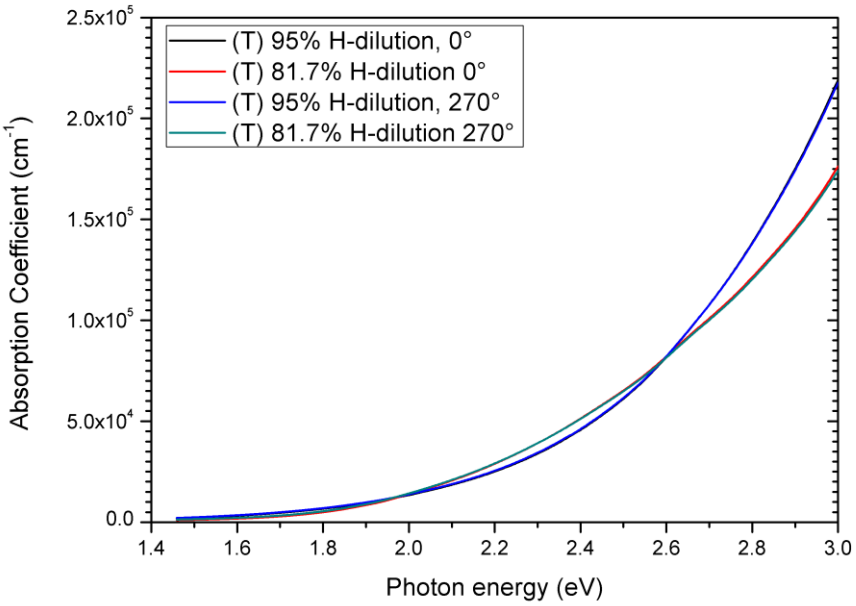

Figure 4.14: Absorption coefficient curves obtained from transmittance spectrum of *nc*-Si:H thin films deposited at 81.7% and 95% hydrogen dilution.

The absorption coefficient was determined directly where the photon energy is 2 eV which is the useful range of the visible spectrum. This correspond to photons energy of wavelength at 620 nm. Table 4.2 present the determined absorption coefficient of the two nanocrystalline thin film at different hydrogen dilution revealing that the absorption coefficient decreases with the increase of the hydrogen dilution. The average absorption coefficient (0° and 270°) for individual nanocrystalline thin films deposited at 81.7% and 95% hydrogen dilutions amounted to 1.40×10^4 cm^{-1} and 1.36×10^4 cm^{-1} respectively revealing that the light absorption of the two nc-Si:H is comparable, and the absorption coefficient value is within the expected order of magnitude i.e. ~ 10^4.

Table 4.2: Absorption coefficient determined from transmittance spectra at 0° and at 270° sample rotations.

Hydrogen dilution	**Spectrum**	**0° ($\times 10^4$ cm^{-1})**	**270° ($\times 10^4$ cm^{-1})**	**Average Absorption coefficient ($\times 10^4$ cm^{-1})**
95%	T	1.34	1.37	1.36
81.7 %	T	1.38	1.42	1.40

As it has already been reported in chapter 3, surface roughness, the thickness and amorphous volume fraction for nc-Si:H with hydrogen dilution 81.7% is relatively higher than nc-Si:H with hydrogen dilution 95%. This may lead to more light being internally reflected and favour the diffuse light scattering at the surface, all of which contribute to the increase in absorption of the light.

4.14.3 DETERMINATION OF FILM THICKNESS

The reflectance spectrum was used to determine the thickness of the film. From the initial fitting parameters, the program calculates the simulated R spectrum together with the associated thickness and the optical constants over the specified energy range. The deviation of the simulated spectra from the measured spectra results were in the 'good' to 'excellent' categories. The extracted thicknesses from the reflectance spectra at respective hydrogen dilution is presented in table 4.3.

Table 4.3: Determined thickness (nm) for the respective sample hydrogen dilution.

Hydrogen dilution (%)	Spectrum	0°	270°	Average
95	R	460.3	453.2	456.8
81.7	R	1910.9	1905.4	1908.2

The determined thickness of nanocrystalline thin film deposited at 95% hydrogen dilution was 456.8 nm compared to 1905.4 nm determined at 81.7% hydrogen dilution. These results agree with the absorption coefficient reported in section 4.11.2 which shows that thicker sample exhibits stronger absorption. It is also observed that the optical thickness of nc-Si:H sample with 95% hydrogen compares well with the physical thickness determined from SEM on the silicon substrate i.e. 455 $\pm$ 10 nm. However, this was not the case for sample deposited at 81.7% hydrogen dilution. A physical thickness of 1464 $\pm$ 10 nm and a chemical thickness of 1550 nm was reported from SEM and TOF-SIMS respectively which is in the same order of magnitude to the determined optical thickness. This observation may be attributed to variation in surface roughness of the two films. It has been confirmed from AFM that surface roughness on the nanocrystalline thin film deposited at 81.7% is relatively higher than nanocrystalline thin film deposited at 95%. As a result, the incident light is diffusely reflected off the surface in many directions and influencing the measured specular reflectance component and distorts the spectrum compared to the other sample.

4.14.4 DETERMINATION OF ENERGY BAND GAP AND REFRACTIVE INDEX

The determination of energy band gap and refractive index was obtained from the specular reflectance spectrum measurements. Detailed analysis was performed using the model suggested by Wemple and Didomenico [4.29]. The value of dispersion parameters i.e. E_0, E_d and static refractive index n_0 were determined from the linear fitting parameters of the graphs in figure 4.15. Summarized values of the dispersion parameters calculated from equation 4 are depicted in table 4.4.

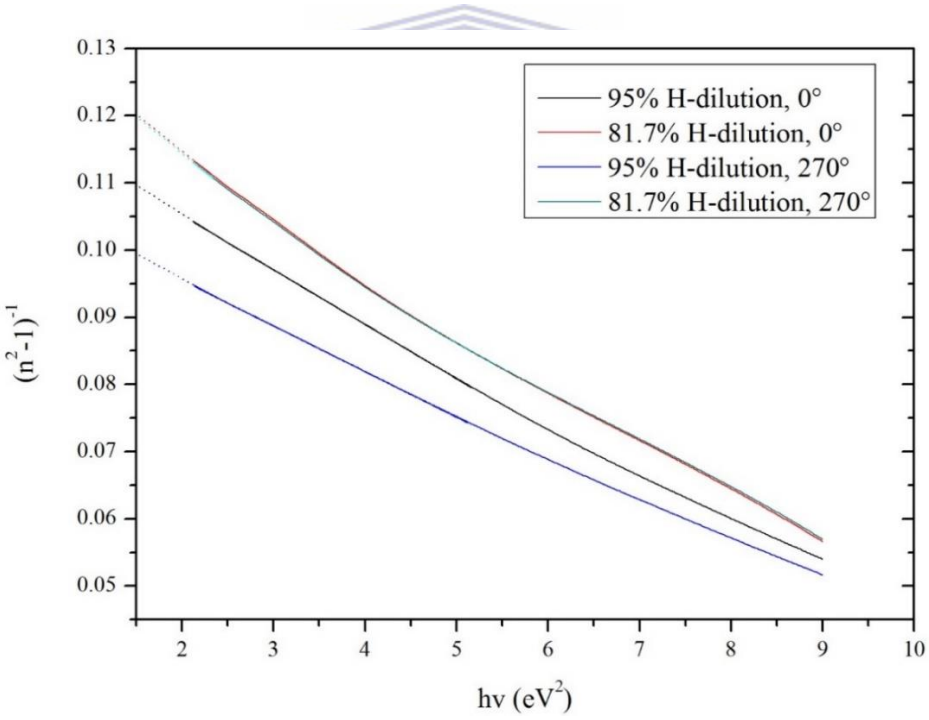

Figure 4.15: Extrapolation of refractive index data obtained from specular reflectance spectrum.

Table 4.4: Calculated values of dispersion parameters and static refractive index.

Hydrogen dilution (%)	Orientation	E_0 (eV)	$E_0/2$ (eV)	E_d	n_0	Ave (n_0)
95	0°	3.87	1.94	31.89	3.04	3.07
95	270°	3.97	1.98	34.01	3.09	
81.7	0°	3.71	1.86	27.78	2.92	2.92
81.7	270°	3.72	1.86	27.99	2.92	

The obtained values of E_0 measured at 0° increases from 3.71 to 3.87 with increasing hydrogen dilution and the values measured at 270° increases from 3.72 to 3.97 with the increase in hydrogen dilution. As explained by Tanaka [4.43], the oscillator energy (E_0) is an average energy gap and to a good approximation, scales with the optical band gap (E_g) i.e. $E_0 \approx 2E_g$. The calculated values of band gap energy (E_g) using this argument are given in table 4.6. The approximated values calculated from the modelling of the spectra measured at 0° are 1.86 and 1.94 eV at 81.7% and 95% hydrogen dilutions respectively. The values obtained at 270° are 1.86 and 1.98 eV for 81.7% and 95% dilutions respectively.

Depending on the process parameters, the typical band gap values of *a*-Si:H are expected to lie between 1.6 and 1.7 eV, whereas 1.1 eV is reported for crystalline silicon [4.44]. In the case of hydrogenated nanocrystalline silicon which is a mixed phase of crystalline and amorphous the band gap value lies normally at 2 eV or much higher. Nevertheless, the calculated energy gap values are consistent with the predicted Tauc energy gap values for amorphous and nanocrystalline material. These values confirm that the sample deposited at 95% hydrogen dilution exhibit the optical properties of a nanocrystalline thin film. The bandgap > 1.7 eV for sample deposited at 81.7% dilution indicates that the material is in transition to the

nanocrystalline phase. Also shown in Table 4.4 is the average refractive index at different hydrogen dilutions. Comparison of the two nc-Si:H shows that the refractive index n_0 increases on average from 2.92 to 3.07 with the increase in the hydrogen dilution ratio. The refractive index n(m) of a material is directly related to the density [4.45]. Theoretically, the light wave bends more when travelling through the material with high density. Thus, dense material exhibits relatively higher refractive index (n_0) values. The results obtained from XRD, Raman and HRTEM analysis have already confirmed that the nc-Si:H deposited at 95% hydrogen dilution has a high crystalline volume fraction, hence denser than the nc-Si-H deposited at 81.7%. The increased refractive index due to the increase in crystallite size and coalescence of smaller nano-crystallites have also been reported in the work done by Arendse et.al [4.46]. The low refractive index observed at nc-Si-H deposited at 81.7 % is due to the more disordered and porous material.

4.15 CONCLUSION

The reflectance and transmittance spectra of the *nc*-SiH thin films has been successfully measured using distinct double beam UV-VIS spectrophotometers. Through traceability, the respective spectra could be compared and used in the modelling of the optical functions. This was possible by using a traceable calibrated reflectance standard to perform the baseline measurements of the instruments. The study has proven that the UV-VIS technique, could be used as a fast and inexpensive method of characterising nc-Si:H thin films. Interference patterns maybe used to predict the thickness of the sample. Fewer interference fringes indicate a thin sample whilst more interference implies thicker sample. A prior attempt to use a virtual film made up of 3 layers with varying features (i.e. voids, crystals, a-Si) could not allow accurate fitting of the spectra. Thus, the accuracy of the fitting was improved by using 6 layers

in the virtual film. The optical thickness of the nanocrystalline thin film deposited at 95% hydrogen dilution (457 nm) corresponds well with SEM (455 nm) and HRTEM (466 nm). However, the optical thickness for nanocrystalline thin film deposited at 81.7 % (1908 nm) is higher than that predicted in chapter 3. Although the thickness is in the same order of magnitude, it is slightly higher than what is predicted by SEM (1461 nm), HRTEM (1467 nm) and TOF-SIMS (1450nm). Surface roughness and the non-uniformities at the sampling area distorting the spectra were attributed to be the cause this observation. The evolving structural features due to the variation in hydrogen dilution influences the optical properties of the nanocrystalline thin film material. The transmittance spectra reveal a blue shift of absorption edge with increasing hydrogen dilution. This shift was attributed to the quantum confinement effects. The increased number of nanosized crystallites with hydrogen dilution which lead to quantum confinement effect was confirmed by Raman spectroscopy and XRD results.

Specular reflectance spectrum shows an increased reflectance intensity at high photon energies and the effect is more with hydrogen dilution confirming that nanocrystalline thin film deposited at 95% has more crystalline components. The absorption coefficient decreases with the increase in hydrogen dilution confirming that nanocrystalline deposited at 81.7 % hydrogen dilution is relatively amorphous. The static refractive index n_0 increases with hydrogen dilution, revealing that 95% has a high crystalline volume fraction as confirmed by the results from XRD, Raman and HRTEM and denser relative to the 81.7% hydrogen dilution sample. The density of material affects the refractive index. The determined energy gap value confirms that 81.7% is amorphous and 95% is nanocrystalline. These values are consistent with the predicted Tauc values. The nano-sized crystallites lead to the widening of the band gap at the beginning growth stages of the film due to the quantum confinement effect.

4.16 REFERENCES

[4.1] E. Vallat-Suavain, U. Kroll, J. Meier, N. Wyrsch, A. Shah (2000) J. Non-Cryst. Solids 266-269:125.

[4.2] S. Halindintwalia et al (2009). Synthesis of nanocrystalline silicon thin films using the increase of the deposition pressure in the hot-wire chemical vapour deposition technique, South African Journal of Science 105.

[4.3] S. Furukawa and T. Miyasato (1988), Quantum size effects on the optical band gap of microcrystalline Si:H, *Physical Review B*, vol. 38, no. 8, pp. 5726–5729.

[4.4] W. Li, D. Xia, H. Wang, and X. Zhao (2010), Hydrogenated nanocrystalline silicon thin film prepared by RF-PECVD at high pressure, *Journal of Non-Crystalline Solids*, vol. 356, no. 44-49, pp. 2552–2556.

[4.5] A. H. Mahan et.al (2004), On the influence of short and medium range order on the material band gap in hydrogenated amorphous silicon, *Journal of Applied Physics*, vol. 96, no. 7, pp. 3818–3826.

[4.6] K. Bhattacharya and D. Das (2007), Nanocrystalline silicon films prepared from silane plasma in RF-PECVD, using helium dilution without hydrogen: structural and optical Characterisation, *Nanotechnology*, vol. 18, no. 41, Article ID 415704.

[4.7] C. J. Oliphant et al (2011). Growth kinetics of nc-Si:H deposited at 200 °C by hot-wire chemical vapour deposition, Thin Solid Films 519:4437–4441.

[4.8] S. Halindintwali (2005), A study of hydrogenated nanocrystalline silicon thin films deposited by hot – wire chemical vapour Deposition (HWCVD). PhD thesis. University of the Western Cape, Cape Town, South Africa.

[4.9] C. J. Oliphant (2012), Hot-wire chemical vapour deposition of nanocrystalline silicon and silicon nitride: growth mechanisms and filament stability. PhD thesis. University of the Western Cape, Cape Town, South Africa.

[4.10] K. F. Feenstra, R. E. I. Schropp, W. F. van der Weg (1999) J. Appl. Phys. **85**:6843.

[4.11] N. A. Bakr et al., (2011) J. Phys. Chem. Solids 72:685.

[4.12] N. A. Bakr et al (2011), Determination of the optical parameters of a-Si:H thin film deposited by Hot wire-chemical vapour deposition techniques using transmission spectrum only, Pramana Indian Academy of Science vol 76, No.3 Journal of Physics,pp. 519-531.

[4.13] J. C. Travis, M. V. Smith, S. D. Rasberry, and G. W. Kramer (2000) NIST SPECIAL PUBLICATION 260-140, Standard Reference Materials, Technical Specifications for Certification of Spectrophotometric NTRMs.

[4.14] J. A. Russell (2011), Measurement of Optical Bandgap Energies of Semiconductors. MSc thesis, Oregon State University, Corvallis, USA.

[4.15] M Bass (Ed) et.al (1995), Handbook of optics, Devices, Measurement & Properties (Second Edition), Volume II, ISBN 0-07-047974-7.

[4.16] V. Lucarini, J.J Saarinen, K.E Peiponen, E.M Vartiainen (2005), Kramers-Kroning Relations in optical Materials Research, ISBN-10 3-540-23673-2 Springer, Heidelberg, New York.

[4.17] Optical Society of America (2010), Handbook of optics (3rd edition), 5 volume set, ISBN: 0071753427, 9780071753425, McGraw-Hill Professional.

[4.18] F. Wooten (1972), Optical Properties of Solids, Academic Press, Inc.

[4.19] Z. Remeš (1999), Study of defects and microstructure of amorphous and microcrystalline silicon thin films and polycrystalline diamond using optical methods. PhD thesis. Charles University, Prague, Czech Republic.

[4.20] R. A. Street (1991), Hydrogenated Amorphous Silicon, Cambridge Solid State Science Series, Cambridge.

[4.21] Thin-film solar cells, TU delft open course ware, Accessed on January 2018, from https://ocw.tudelft.nl/course-readings/solar-cells-r5-thin-film-silicon/.

[4.22] I. Chambouleyron, J. M. Martínez, H. S. Nalwa (ed) (2001), *Handbook of Thin Films Materials,* volume 3, Chapter 3, Academic Press, the University of Michigan.

[4.23] W. M Bullis, D. G Seiler, A.C Diebold (1996), Semiconductors Characterisation, American Institute of Physics.

[4.24] S. K. O'Leary, S. R Johnson, P. K Lim (1997), The relationship between the distribution of electronic states and the optical absorption spectrum of an amorphous semiconductor: an empirical analysis, J. Appl. Phys. 82 (7).

[4.25] T. Söderström (2009), Single and multi-junction thin film silicon solar cells for flexible PVs. PhD thesis. University of Neuchâtel, Neuchâtel, Switzerland.

[4.26] M. Elahi, D. Souri (2006), Study of optical absorption and optical band gap determination of thin amorphous TeO2-V2O5-MoO3 blown films, Indian Journal of Pure & Applied Physics, Vol. 44, pp. 468-472.

[4.27] E. Kim, Z. Jiang, K. No (2000), Measurement and Calculation of Optical Band Gap of Chromium Aluminum Oxide Films, Jpn.J.Appl.Phys.vol 39, pp (4820-4825).

[4.28] E. F. Schubert (2006), Light-Emitting Diodes, 2nd edition: Cambridge University Press.

[4.29] S. H. Wemple, M. Didomenico (1971), Phys. Rev. B3, 1338, DOI: 10.1103/PhysRevB.3.1338.

[4.30] S. Jacobs et.al (2012), Optical properties of SiN:H thin films obtained by hydrogen dilution, ISBN: 978-1-77592-070-0, Proceedings of SA Institute of Physics Conference.

[4.31] R. SWANEPOEL (1983), Determination of the thickness and optical constants of amorphous silicon, Journal of Physics E: Scientific Instruments 16(12), pp. 1214–1222.

[4.32] F. Wooten (1972), Optical properties of solids, Academic press: 72-187257.

[4.33] S. K. O'Leary, S.R. Johnson, P.K. Lim (1997), J. Appl. Phys. 82 (7) 3334.

[4.34] W. Theiss (2008), Hard and software for optical spectroscopy, http://www.wtheiss.com

[4.35] J. A. Sap (2010), Modelling optical properties of layers for thin film silicon solar cells, MSc. Thesis, Delft University of Technology, Netherlands.

[4.36] D. Stroud (1998), The effective medium approximations: Some recent developments Superlattices and Microstructures, Vol. 23, No. 3/4, The Ohio State University, Columbus, OH 43210-1106, U.S.A.

[4.37] S. Bosch et al. (2000), Effective dielectric function of mixtures of three or more materials: a numerical procedure for computations Surface Science 453: 9–17.

[4.38] J. C. Maxwell Garnett, Phil. Trans. R. Soc. Lond, A (1904) 203.

[4.39] D. A. G. Bruggermann (1935), Ann. Physik (Leipzig), **24:** 636.

[4.40] D. E. Aspens (1982), Local-field effects and effective-medium theory: A microscopic perspective, Am. J. phys, 50(8).

[4.41] N. A. Tarjudin, I. Sumpono, S. Sakrani (2012), Optical Properties of Nanocrystalline Silicon Thin Films in Wider Regions of Wavelength, Journal of Science and Technology, Vol 4 No 1.

[4.42] T.F.G. Muller (2009) Optical model of amorphous and Metal Induced Crystallized silicon with an effective medium approximation. PhD thesis. University of the Western Cape.

[4.43] K. Tanaka (1980), Thin Solid Films **66**, 271.

[4.44] V. S. Waman et.al (2011), Hydrogenated nanocrystalline silicon thin films prepared by hot wire method with varied process pressure, Journal of Nanotechnology, volume 2011, DOI: 10.1155/2011/242398.

[4.45] E.C. Freeman, W. Paul (1972), Phys. Rev. B 5, 3017, DOI: 10.1103/PhysRevB.5.3017.

[4.46] C. J. Arendse et.al (2009), Thermally Induced Nano-Structural and Optical Changes of nc-Si:H Deposited by Hot-Wire CVD, Nanoscale Res Lett 4:307-312, DOI 10.1007/s11571-008-9243-0.

CHAPTER 5

A SUMMARY

The modelling of the *nc*-Si:H transmittance and reflectance spectra was successfully achieved by using SCOUT® software. This work extends the built-in capabilities of the Scout® software such that material description in the software program correlates more clearly with the actual physical material under investigation. The relationship between the nano-structural and the chemical, electronic and optical properties of an nc-Si:H thin film synthesised by hot-wire CVD was investigated. Secondary ion mass spectrometry depth profiling was used to track the presence of porosity and the incubation layer. HRTEM analysis reveals a film with porosity that decrease in extent moving from the incubation layer to the film surface. The nanocrystals formed within micron-sized crystalline cone regions and their size increased moving along the growth direction. The electronic structure of the nc-Si:H varies along the growth direction of the film and was influenced by the crystallinity, porosity and the chemical composition (H- and O-content). An optical model was developed based on the nano-structural and chemical properties of the nc-Si:H film to extract an optical thickness based on UV–Vis measurements.

Analysis of optical thickness for the nanocrystalline thin film deposited at 95% hydrogen dilution correspond well with the physical and chemical thickness obtained from SEM and HRTEM respectively. However, the optical thickness derived from nanocrystalline thin film deposited at 81.7% nanocrystalline thin film agrees to an order of magnitude to the thickness determined from TOF-SIMS, SEM and HRTEM, but was not as closely in agreement compared to the 95% dilution sample. This was attributed to surface roughness and non-uniformity on

the area where the thin film sample was obtained. The optical band gap agrees with the theoretical Tauc band gap revealing that thin film deposited at 95% hydrogen dilution is more nanocrystalline. The refractive index increases with the hydrogen dilution revealing increased density of the material with hydrogen dilution. The light scattering due to a rough surface and bulk inhomogeneity is of crucial importance for solar cell thin films. Scattering effects leads to an improved absorption of light. In this study, it has been shown that complex nanostructured materials such as nc-Si:H can be accurately characterised by considering a combination of techniques probing the material from the atomic to the micron scale. The careful correlation between independent techniques provides a better understanding of the growth and properties of the nanomaterial. This shows that there is yet opportunity to improve on the analysis of well-established research materials.

Suggested further work is the determination of (rms) roughness and Haze factor from the reflectance spectra using scalar scattering theory suggested by Bennet and Porteus [5.1]. This approach requires accurate determination of beam's angle of incident. The possibility of using reflectance spectra to determine the (rms) roughness value of the *nc*-Si:H thin film could be validated by AFM. The determined (rms) roughness may also be used to correlate surface features such as crystallinity and density as obtained from XRD and Raman spectroscopy. On the other hand, haze meter for measuring haze factor of *nc*-Si:H thin film need to be considered as this could provide a solution for rapid determination of (rms) roughness.

5.1 REFERENCES

[5.1] H.E. Bennett and J.O. Porteus (1961), Relation between surface roughness and specular reflectance at normal incidence, J. Opt. Soc. Am. 51(2), 123–129 (1961)